RSC Advances

PAPER

View Article Online
View Journal | View Issue

Cite this: *RSC Adv.*, 2019, **9**, 36208

Co(OH)F nanorods@K_xMnO_2 nanosheet core–shell structured arrays for pseudocapacitor application

Si Chen,[a] Yi Song,[b] Xuejiao Zhou[a] and Mingyi Zhang *[a]

Received 3rd September 2019
Accepted 28th October 2019

DOI: 10.1039/c9ra07024a

rsc.li/rsc-advances

In this work, Co(OH)F nanorods@K_xMnO_2 nanosheet core–shell nanostructure was assembled on Ni foam by a facile hydrothermal method and incorporated with an electrodeposition process. Benefiting from their core–shell nanostructure and heterogeneous nanocomposites, the arrays present high areal capacitance up to 1046 mF cm^{-2} at 1 mA cm^{-2} and display a remarkable specific capacitance retention of 118% after 3000 cycles. When the current density increases to 10 mA cm^{-2}, the capacitance is 821 mF cm^{-2} displaying a good rate capability. The excellent electrochemical properties allow them to be used as a promising electrode material for pseudocapacitors and display wide application potential in the field of electrochemical capacitors.

1 Introduction

At present, the energy crisis and environmental pollution continue to increase, forcing people to develop new energy storage equipment. Supercapacitors, devices with high power density and long cycle life, come into being.[1–5] As everyone knows electrode materials are very important for the application of supercapacitors.[6–10] Varieties of materials involving conductive polymers, carbon, and transition metal oxides/hydroxides have been reported as electrodes for supercapacitors, but, oxides/hydroxides are very popular in energy storage devices because of their multiple oxidation states leading to reversible faradaic reactions.[11–14] Unluckily, inherently low electric conductivity and short diffusion distance cause an unsatisfactory supercapacitor performance such as poor cycling life.[15] Therefore, an effective tactic is produced by combining diverse metal oxides/hydroxides to design hybrid structures. The hybrid structures have numerous competitive edges for instance rich and accessible electroactive sites, high electron/ion diffusion efficiency, superior rate performance and improved cycle life as the result of the synergistic effect through the reinforcement or modification of the multiple components.[16,17] Hence, hybrid electrodes can take advantage of both components and offer special properties through the reinforcement or modification of each other. So, a series of hybridized structures such as, β-$Co(OH)_2$/Co(OH)F, $Ni(OH)_2$/CNs, $NiCo_2O_4$@AMCRs, *etc.* have been widely investigated.[18–22]

Another way is to fabricate electrodes with a distinct architecture, for example, core–shell structure directly grown on the conductive substrates forming a binder-free electrode. In this novel heterogeneous core–shell structure, both "core" and "shell" electrochemical materials can be fully utilized and have a good synergetic effect. What's more, direct growing on the conductive substrate avoids the electrical resistance of the binder and promotes fast electron transport to conductive substrate that enhance the electrochemical properties of the electrode.

In this study, we report on the design of an advanced electrode architecture of Co(OH)F nanorods@K_xMnO_2 nanosheets core–shell structure grown on Ni foam by a hydrothermal method and incorporated with an electrodeposition process, where the shell were interconnected on the core forming a highly porous and open structure and firmly adhered to the substrate. The presence of K^+ in shell material develops a Co(OH)F/K_xMnO_2 core–shell structure as electrodes for supercapacitors. These arrays were further investigated with respecting to their application as electrodes for supercapacitors. Excitingly, comparing with the pure Co(OH)F nanorods and K_xMnO_2 nanosheets, the Co(OH)F nanorods@K_xMnO_2 nanosheets core–shell arrays with higher capacitance exhibit noticeable electrochemical performance and good cycling stability. Remarkably, the bicomponent nanostructure displays high areal capacitance, great rate capability and fantastic cycling stability in the supercapacitor applications.

2 Experimental and computational section

2.1 Materials synthesis

Synthesis of Co(OH)F nanorods. A piece of Ni foam (1 × 1.5 cm^2) was fully cleared with hydrochloric acid, absolute acetone, ethanol and deionized water under ultrasonic for 20 min, respectively, before used. For the synthesis of Co(OH)F nanorods, firstly, 0.374 g $Co(CH_3COO)_2 \cdot 4H_2O$ and 0.052 g LiF were

[a]*Key Laboratory for Photonic and Electronic Bandgap Materials, Ministry of Education, School of Physics and Electronic Engineering, Harbin Normal University, Harbin 150025, PR China. E-mail: zhangmingyi@hrbnu.edu.cn; mysci@foxmail.com*

[b]*Institute of Data Science and Artificial Intelligenc, Harbin Huade University, Harbin 150025, PR China*

added in 30 mL deionized water ultrasonic vibrating to form a dispersed uniform solution. Then, the mixture and the prepared Ni foam (NF) were transferred into a Teflon-lined stainless-steel autoclave and heated at 200 °C for 24 h. Afterward, the obtained Co(OH)F nanorods on the Ni foam (Co(OH)F/NF) were flushed with ethanol and deionized water.

Synthesis of Co(OH)F nanorods@K_xMnO_2 nanosheets core–shell structured arrays. The Co(OH)F nanorods@K_xMnO_2 nanosheets core–shell structured arrays were prepared by the electrodeposition method. In detail, the Co(OH)F nanorods as working electrode, a graphite electrode as counter electrode, 0.02 M manganous acetate and 0.2 M potassium sulphate as the electrolyte. The K^+-inserted MnO_2 was electrodeposited on the Co(OH)F nanorods forming the Co(OH)F nanorods@K_xMnO_2 nanosheets core–shell structure at 4.0 mA cm^{-2} for 10 min at room temperature.

Synthesis of K_xMnO_2 nanosheets. The experimental conditions of K_xMnO_2 nanosheets deposition on the Ni foam (K_xMnO_2/NF) are the same as that of on the Co(OH)F nanorods.

2.2 Physical characterizations

The scanning electron microscope (SEM, Hitachi, SU70), energy-dispersive X-ray spectroscopy (EDX) and transmission electron microscope (TEM, FEI, Tecnai TF20) were used for the investigation of microstructure.

2.3 Electrochemical measurements

The electrochemical measurements were carried out by a three-electrode system in 0.5 M LiOH and 3 M KOH mixed solution. Co(OH)F nanorods, Co(OH)F nanorods@K_xMnO_2 nanosheets core–shell structure and K_xMnO_2 nanosheets on the NF as working electrodes, respectively. The area of the working electrodes mentioned above submerged into the electrolyte was steered at about 1 cm^2. The electrochemical calculation was steered with an electrochemical workstation (VMP3, France). A Pt foil and Hg/HgO electrode were used as the counter electrode and reference electrode, respectively. And all the experiments were conducted at ambient temperature. At various scanning rates, the cyclic voltammetry curve (CV) could be obtained in the potential range of 0–0.6 V. The galvanostatic charge/discharge (GCD) processes were accomplished at various current densities in 0 to 0.56 V. Electrochemical impedance spectroscopy (EIS) is calculated by using an AC voltage of 5 mV amplitude over a frequency range of 0.01 Hz to 100 kHz. Under the condition of current density of 10 mA cm^{-2}, the stability of 3000 cycles was estimated by CV measurement. According to the following eqn (1), we can calculate the areal capacitances of the working electrode:

$$C = \frac{I\Delta t}{s\Delta V} \quad (1)$$

where I, t, S and V are the constant discharge current, discharge time, geometrical area and potential window of the electrode respectively. According to the following eqn (2), we can calculate the diffusion coefficient of electrolyte ions at the interfacial region:

$$D = (2^{-1/2}RTn^{-2}F^{-2}A^{-1}\sigma^{-1}C^{*-1})^2 \quad (2)$$

where R, T, n, F, A, σ and C^* are the gas constant represents, absolute temperature, charge-transfer number, Faraday constant, area of the working electrode, Warburg coefficient and concentration of the electrolyte, respectively.

3 Results and discussion

The scanning electron microscopy (SEM) images of the Co(OH)F nanorods grown on Ni foam are displayed in Fig. 1a and b. Distinctly, slim Co(OH)F nanorods with sharp tips joining together form a firewood-pile-like bundle and homogeneously align on the NF. The insert in Fig. 1a shows the surface of pure NF that is clean and smooth. In Fig. 1b, the diameter of a single nanorod is mainly between 50 nm and 170 nm. After the electrodeposition, it is evident that the nanorods gathering in a pile are scattered and separated apart adequately on the Ni foam (Fig. 1c and d). Of importance, some nanosheets grow on the Co(OH)F nanorods forming a core–shell structure. The nanosheets are proved to the K_xMnO_2 nanosheets in the next discussion. To assess the uniformity of the K_xMnO_2 nanosheets grown on the Co(OH)F nanorods, elemental mapping analysis was conducted by SEM. Fig. 2 represents the SEM image and the corresponding elemental mapping of the Co(OH)F nanorods@K_xMnO_2 nanosheets core–shell structure. The Mn, O, and K maps are analogous to those of the original SEM image, indicative of a uniformity K_xMnO_2 nanosheets on the Co(OH)F nanorods. Structural information of the Co(OH)F nanorod and the Co(OH)F@K_xMnO_2 composited products are further investigated by transmission electron microscopy (TEM).

Fig. 3a displays that an individual Co(OH)F nanorod is gotten by ultrasound in ethanol. The nanorod has a relative smooth surface that in accord with the result of SEM. Fig. 3b reveals the high-resolution TEM image of Co(OH)F nanorod, a fringe spacing of 0.265 nm can be indexed as the lattice space

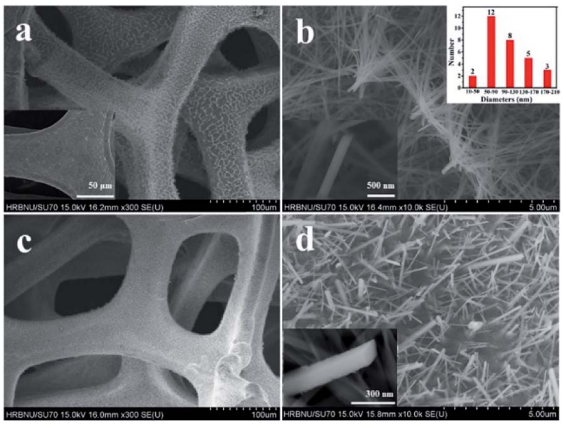

Fig. 1 Typical SEM image of the Co(OH)F nanorods on Ni foam at (a) low and (b) high magnifications, the insert is the SEM image of the pure Ni Foam and the size distribution of the diameters of the nanorods in (a) and (b) typical SEM image of the Co(OH)F@K_xMnO_2 core–shell structure on Ni foam at (c) low and (d) high magnifications.

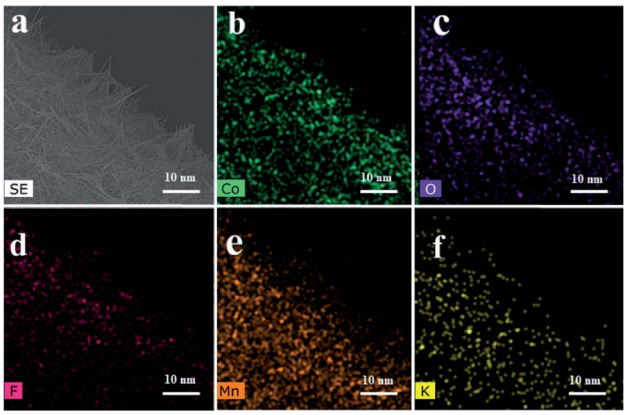

Fig. 2 (a) SEM image and corresponding element mapping (b–f) using cobalt Co, oxygen O, fluorine F, manganese Mn and potassium K of Co(OH)F@K_xMnO_2 core–shell structure.

of (201) of Co(OH)F. Fig. 3c exhibits the TEM images of Co(OH)F@K_xMnO_2 core–shell structure. It is also clear that the Co(OH)F@K_xMnO_2 nanorod shows a core–shell structure, and the surface of Co(OH)F nanorod (the dark-colored region) is surrounded by K_xMnO_2 nanosheets (the light-colored region). A high-resolution TEM image of the K_xMnO_2 nanosheets in core–shell structure is presented in Fig. 3d, interplanar spacing of 0.34 nm, corresponds well to that of (002) plane of MnO_2.[23] Also, for purpose of more clear to study the Co(OH)F@K_xMnO_2 core–shell structure and composition distribution, the TEM-EDX analysis is employed. Fig. 4 displays the spatial distribution of the compositional elements within the core–shell structures by line scans along the nanorod's radial direction (marked by the orange line). The TEM-EDX mappings indicate that the core–shell structure distributes five elements of Co, F, K, Mn and O, meanwhile, the strongest signals for Co, F and O are observed in the backbone area, but only Mn and O signals are found in the shell area, implying the successful synthesis of core–shell structure.

Next, we directly apply the Co(OH)F@K_xMnO_2 core–shell structured on NF as an integrated electrode to examine the electrochemical properties of the unique structure in a three-electrode system and 0.5 M LiOH and 3 M KOH as the electrolyte. Fig. 5a exhibits the typical CV curves of the Co(OH)F nanorods, K_xMnO_2 nanosheets, Co(OH)F@K_xMnO_2 core–shell structure supported on NF and pure NF in a potential window of 0 to 0.6 V at a scan rate of 100 mV s^{-1}. The Ni foam almost has little CV curve area compared with the other electrodes, indicating a low capacitance. Obviously, a pair of redox peaks can be found for the Co(OH)F electrode, implying the presence of faradaic reactions that related to the valence change of Co ions in alkaline solution.[24,25] Meanwhile, the core–shell structure has a much larger CV-integrated area than the Co(OH)F nanorods and K_xMnO_2 nanosheets, revealing a much higher areal capacity. That confirms the additional pseudocapacitance contribution of K_xMnO_2 as a shell to the total.[26,27]

The GCD curves of the three electrodes are presented in Fig. 5b and these are recorded at a current density of 2 mA cm^{-2} with potential window of 0–0.56 V. The three electrodes all exhibits typical pseudocapacitive behavior with distinct plateau regions consistent with the redox reaction peaks of CVs.[28] In the GCD curves, the sample of Co(OH)F@K_xMnO_2 core–shell structure owns the longest discharge time among three samples that means Co(OH)F@K_xMnO_2 core–shell structure having the largest capacitance according to the eqn (1). Fig. 5c shows the Nyquist plots of the three electrodes. In the Nyquist curves, the charge transfer resistance (R_{ct}) of the Co(OH)F@K_xMnO_2 core–shell structure on Ni foam is about 1.309 Ω that shows a good charge transport. In the low frequency region, the slope of inclined line stands for diffusion resistance, which arises as a consequence of frequency reliant ion transportation in the electrolytes. The slope of inclined line is higher, the ion diffusion rate is larger in the material.[29] Obviously, the inclined line of the Co(OH)F@K_xMnO_2 core–shell structure and Co(OH)F nanorods are similar and both larger than K_xMnO_2 nanosheets indicating better ion diffusion rate. The EIS data is used to obtain the diffusion coefficients (D) of the three electrodes for electrolyte ions.[30] The diffusion coefficients, got by the Randles plot (Fig. 5d) using eqn (2), come out to be 4.46×10^{-9}, 1.81×10^{-9} and 7.78×10^{-9} cm^2 s^{-1} for Co(OH)F, K_xMnO_2 and Co(OH)F@K_xMnO_2 samples, respectively. From this result it is clear that the Co(OH)F@K_xMnO_2 core–shell structure is the best performer among all the samples in the present work.

We have further studied its specific electrochemical behavior. Fig. 6a displays the typical cyclic voltammograms (CVs) of the Co(OH)F@K_xMnO_2 nanocomposite electrodes that are conducted at various scan rates 5–100 mV s^{-1} with a potential range between 0 V and 0.6 V. All the CV curves show a pair of strong redox peaks, implying that the capacitance characteristics are mainly governed by faradaic redox reactions. When the scan rate is increasing, the peak current is boosting linearly, suggesting that rapid kinetics of the interfacial faradaic

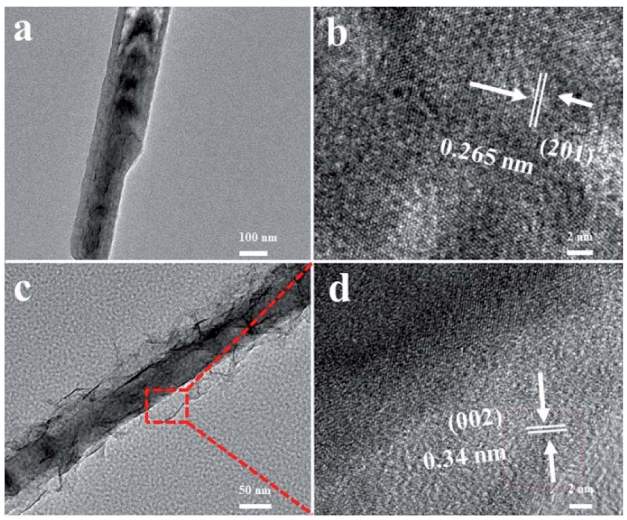

Fig. 3 (a) TEM image of Co(OH)F nanorods; (b) HRTEM images of the Co(OH)F nanorods; (c) TEM image of Co(OH)F@K_xMnO_2 core–shell structure; (d) HRTEM images of the Co(OH)F@K_xMnO_2 core–shell structure.

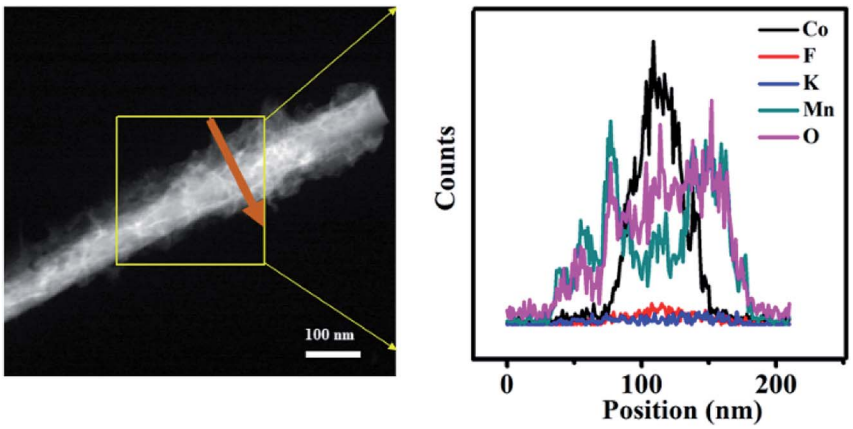

Fig. 4 The representative EDX line scanning spectroscopy for a single Co(OH)F@K_xMnO_2 core–shell nanorod.

redox reactions and fast rates of electronic and ionic transportation in the present scan rates.[31] The shape of the CV curves is not very influenced by the increase of the scan rates, implying the improved mass transportation and electron conduction in the host materials.[32] The galvanostatic charge–discharge measurements are further studied in Fig. 6b at various current densities 1–10 mA cm^{-2} with the voltage range between 0 to 0.56 V. In accordance with the CV results, the nonlinearity of the curves suggests the existence of faradaic processes. From the galvanostatic discharge curves, the capacitance values were got by the eqn (1). Impressively, at a current density of 1, 2, 4, 8 and 10 mA cm^{-2}, the Ni foam supported Co(OH)F@K_xMnO_2 core–shell structure indicates high areal capacitance of 1046, 978, 914, 842 and 821 mF cm^{-2}, respectively that confirms the good rate capability of the Co(OH)F@K_xMnO_2 core–shell structure (Fig. 6c). When the discharge current density at 1 mA cm^{-2}, with a roughly measured active mass-loading of 2 mg cm^{-2}, the Co(OH)F@NF displays a high areal capacitance of 1046 mF cm^{-2} (amount to specific capacitance of 523 F g^{-1} at 1 mA cm^{-2}), larger than those reported materials, for instance Co_x-Ni_3–$xSi_2O_5(OH)_4$/C,[33] electrodeposited MnO_2 nanosheet[34] Co–TiN@NG-2/CC[35] and MnO_2–NiO nanoflakes.[36] What's more, in order to examine the electrochemical durability of the electrode material the cyclic stability test is carried. After 3000 continuous cycles (Fig. 6d), we can see that the device remains 118% of its initial capacitance value, signifies a good electrochemical

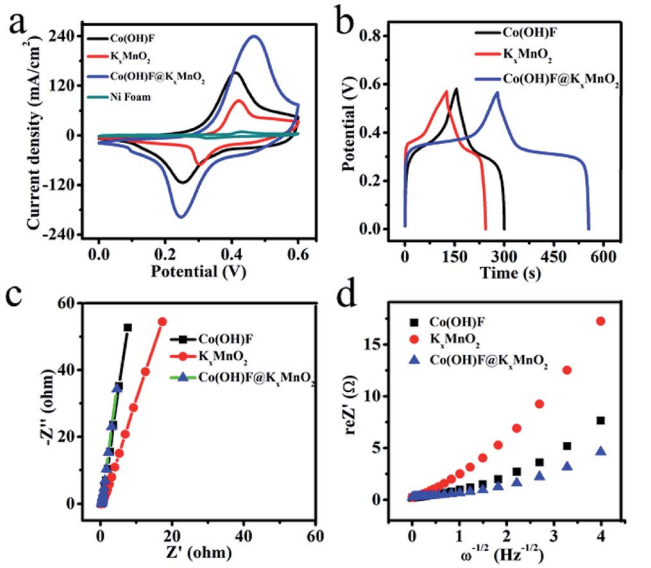

Fig. 5 (a) CV curves of the Co(OH)F nanorods electrode, the K_xMnO_2 nanosheets electrode, the Co(OH)F@K_xMnO_2 core–shell structure electrode and the pure Ni foam at a scan rate of 100 mV s^{-1}; (b) galvanostatic charge–discharge curves of the Co(OH)F nanorods electrode, the K_xMnO_2 nanosheets electrode and the Co(OH)F@K_xMnO_2 core–shell structure electrode at a current density of 2 mA cm^{-2}; (c) and (d) EIS and Randles plots of three synthesized samples.

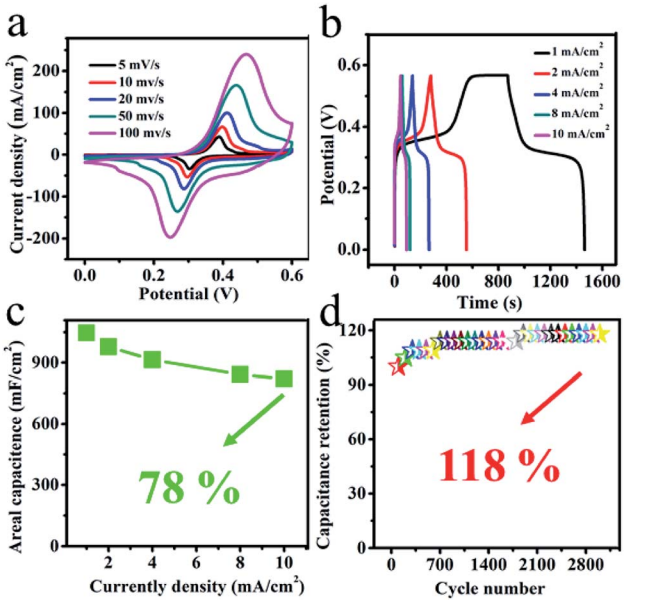

Fig. 6 (a) CV curves of the Co(OH)F@K_xMnO_2 electrode at various scan rates; (b) galvanostatic charge–discharge curves of the Co(OH)F@K_xMnO_2 electrode at various current densities; (c) Areal capacitances as determined from the GCD curves and (d) cyclic stability performance at 10 mA cm^{-2} of the Co(OH)F@K_xMnO_2 electrode.

durability of the material. Noticeably, the specific capacitance has an increase during 1500 cycles and then keep steady that is radically due to an electroactivation process for the electrode.[37]

4 Conclusions

In general, the Co(OH)F@K_xMnO_2 core–shell arrays grown directly on Ni foam have been successfully fabricated by a facile hydrothermal process and an electrodeposition process. The core–shell arrays as the electrode materials display a large areal capacitance of 1046 mF cm^{-2} at 1 mA cm^{-2}, and also present high specific capacitance retention of 118% after 3000 cycles at a constant current density of 10 mA cm^{-2}. Above dates manifest that the core/shell arrays nanocomposites with the enhanced electrochemical performance would provide great potential for energy storage.

Conflicts of interest

There are no conflicts to declare.

Acknowledgements

This work was supported by the National Natural Science Foundation of China (51872068), Heilongjiang Natural Science Foundation (E2018051).

References

1 J. Tang, S. B. Ni, D. L. Chao, J. L. Liu, X. L. Yang and J. B. Zhao, *Electrochim. Acta*, 2018, **256**, 709.
2 G. F. Chen, X. X. Li, L. Y. Zhang, N. Li, T. Y. Ma and Z. Q. Liu, *Adv. Mater.*, 2016, **28**, 7680.
3 H. M. Zhu, Q. Liu, J. J. Liu, R. M. Li, H. S. Zhang, S. X. Hu and Z. S. Lia, *Electrochim. Acta*, 2015, **178**, 758.
4 H. C. Tao, S. C. Zhu, X. L. Yang, L. L. Zhang and S. B. Ni, *Electrochim. Acta*, 2016, **190**, 168.
5 Y. F. Zhang, H. M. Jiang, Q. S. Wang and C. G. Meng, *Chem. Eng. J.*, 2018, **352**, 519.
6 Q. F. Zheng, R. S. Xie, L. M. Fang, Z. Y. Cai, Z. Q. Ma and S. Q. Gong, *J. Mater. Chem. A*, 2018, **6**, 24407.
7 C. Chen, D. Yan, X. Luo, W. J. Gao, G. J. Huang, Z. W. Han and Y. Zeng, *ACS Appl. Mater. Interfaces*, 2018, **10**, 4662.
8 Q. S. Wang, Y. F. Zhang, H. M. Jiang, X. J. Li, Y. Cheng and C. G. Meng, *Chem. Eng. J.*, 2019, **362**, 818.
9 Q. S. Wang, Y. F. Zhang, H. M. Jiang and C. G. Meng, *J. Alloys Compd.*, 2019, **534**, 142.
10 D. Wu, T. Xiao, X. Y. Tan, P. Xiang, L. H. Jiang, Z. Kang and P. Tan, *Electrochim. Acta*, 2016, **198**, 1.
11 H. X. Yang, D. L. Zhao, H. Lin, X. M. Tian, X. Y. Han, Y. J. Duan and M. Zhao, *Electrochim. Acta*, 2018, **292**, 468.
12 W. Hong, J. Q. Wang, P. W. Gong, J. F. Sun, L. Y. Niu, Z. G. Yang, Z. F. Wang and S. R. Yang, *J. Power Sources*, 2014, **270**, 516.
13 X. J. Ma, B. Kong, W. B. Zhang, M. C. Liu, Y. C. Luo and L. Kang, *Electrochim. Acta*, 2014, **130**, 660.
14 B. Zhao, S. Y. Huang, T. Wang, K. Zhang, M. F. Matthew, J. B. Xu, X. Z. Fu, R. Sun and C. P. Wong, *J. Power Sources*, 2015, **298**, 83.
15 M. P. Li, F. E. Maher, Y. H. Jee, D. K. Matthew, M. Kristofer, H. S. Wang, Z. J. Zhao and B. K. Richard, *Nano Res.*, 2018, **11**, 2836.
16 X. Wang, H. Xia, J. Gao, B. Shi, Y. Fang and M. Shao, *J. Mater. Chem. A*, 2016, **4**, 18181.
17 M. Kundu, G. Karunakaran, E. Kolesnikov, A. Dmitry, V. Gorshenkov and D. Kuznetsov, *Microporous Mesoporous Mater.*, 2017, **247**, 9.
18 Z. Z. Liang, Z. Y. Yang, Z. H. Huang, J. Qi, M. X. Chen, W. Zhang, H. Q. Zheng, J. L. Sun and R. Cao, *Electrochim. Acta*, 2018, **271**, 526.
19 M. J. Xie, Z. C. Xu, S. Y. Duan, Z. F. Tian, Y. Zhang, K. Xiang, M. Lin, X. F. Guo and W. P. Ding, *Nano Res.*, 2018, **11**, 216.
20 Y. C. Pang, S. Y. Zhang, S. Chen, J. Liang, M. Y. Li, D. W. Ding and S. J. Ding, *Chem.–Eur. J.*, 2018, **24**, 16104.
21 Y. Cheng, Y. F. Zhang and C. G. Meng, *ACS Appl. Energy Mater.*, 2019, **2**, 3830.
22 J. Q. Zheng, Y. F. Zhang, Q. S. Wang, H. M. Jiang, Y. Y. Liu, T. M. Lv and C. G. Meng, *Dalton Trans.*, 2018, **47**, 452.
23 N. Kanaujiya, N. Kumar, A. K. Srivastava, Y. Sharma and G. D. Varma, *J. Electroanal. Chem.*, 2018, **824**, 226.
24 S. Q. Wang, Z. Q. Zhu, P. W. Li, C. H. Zhao, C. J. Zhao and H. Xia, *J. Mater. Chem. A*, 2018, **6**, 20015.
25 S. Ranganatha and N. Munichandraiah, *ACS Omega*, 2018, **3**, 7955.
26 J. Shao, X. Y. Li, Q. T. Qu and Y. P. Wu, *J. Power Sources*, 2013, **223**, 56.
27 B. H. Zhang, Y. Liu, Z. Chang, Y. Q. Yang, Z. B. Wen and Y. P. Wu, *Electrochim. Acta*, 2014, **130**, 693.
28 X. M. Mu, Y. X. Zhang, H. Wang, B. Y. Huang, P. B. Sun, T. Chena, J. Y. Zhou, E. Xie and Z. X. Zhang, *Electrochim. Acta*, 2016, **211**, 217.
29 K. X. Zhao, H. R. Wang, C. C. Zhu, S. Y. Lin, Z. K. Xu and X. T. Zhang, *Electrochim. Acta*, 2019, **308**, 1.
30 C. T. Hsieh, S. M. Hsu, J. Y. Lin and H. S. Teng, *J. Phys. Chem. C*, 2011, **115**, 12367.
31 D. Ghosh, S. Giri and C. K. Das, *Nanoscale*, 2013, **5**, 10428.
32 L. Huang, J. W. Xiang, W. Zhang, C. J. Chen, H. H. Xu and Y. H. Huang, *J. Mater. Chem. A*, 2015, **3**, 22081.
33 Y. F. Zhang, C. Wang, H. M. Jiang, Q. S. Wang, J. Q. Zheng and C. G. Meng, *Chem. Eng. J.*, 2019, **375**, 121938.
34 H. Xia, M. O. Lai and L. Lu, *JOM*, 2011, **63**, 54.
35 Q. Zhu, L. M. Yao, R. Tong, D. Liu, K. W. Ng and H. Pan, *New J. Chem.*, 2019, **43**, 14518.
36 J. P. Liu, J. Jiang, B. Michel and H. J. Fan, *J. Mater. Chem.*, 2012, **22**, 2419.
37 X. D. Li, R. Ding, W. Shi, Q. L. Xu, D. F. Ying, Y. F. Huang and E. H. Liu, *Electrochim. Acta*, 2018, **265**, 455.

